AGU PUBLICATIONS

JGR

Journal of Geophysical Research: Atmospheres

RESEARCH ARTICLE
10.1002/2013JD021350

Key Points:
- Arctic ozone depletion 2011 contributed to tropospheric circulation anomalies
- Ozone impacts are weak in isolation, but they significantly amplify SST forcing
- Nonlinear interactions between ozone and SST forcings implicated in the results

Supporting Information:
- Readme
- Figures S1–S2

Correspondence to:
A. Yu. Karpechko,
alexey.karpechko@fmi.fi

Citation:
Karpechko, A. Yu., J. Perlwitz, and E. Manzini (2014), A model study of tropospheric impacts of the Arctic ozone depletion 2011, *J. Geophys. Res. Atmos.*, *119*, 7999–8014, doi:10.1002/2013JD021350.

Received 24 DEC 2013
Accepted 10 JUN 2014
Accepted article online 13 JUN 2014
Published online 8 JUL 2014

A model study of tropospheric impacts of the Arctic ozone depletion 2011

Alexey Yu. Karpechko[1], Judith Perlwitz[2,3], and Elisa Manzini[4]

[1]Finnish Meteorological Institute, Arctic Research, Helsinki, Finland, [2]Cooperative Institute for Research in Environmental Sciences, University of Colorado Boulder, Boulder, Colorado, USA, [3]Physical Science Division, NOAA/Earth System Research Laboratory, Boulder, Colorado, USA, [4]Max Planck Institute for Meteorology, Hamburg, Germany

Abstract Record Arctic ozone loss in spring 2011 occurred in concert with record positive values of the tropospheric Northern Annular Mode (NAM) index raising the question about the role of stratospheric driver on this tropospheric climate event. A set of 50 years long simulations by atmospheric general circulation model European Centre/Hamburg version 5 (ECHAM5) is carried out and the responses of the model to observed anomalies in stratospheric ozone (O3) and sea surface temperatures (SST) separately and also the response to combined SST and O3 forcing (ALL) are analyzed. In all three experiments the response is characterized by a strengthening of stratospheric polar vortex in March–April. In the ALL experiment, this strengthening is followed by a significant, long-lasting shift of the tropospheric circulation toward a positive NAM phase and increased probability of occurrence of extremely positive NAM events. The combined effect of the O3 and SST forcings on the stratospheric circulation differs from the sum of the individual O3 and SST responses, most likely due to nonlinear effects, leading to a colder stratosphere in February–March. In the troposphere, the sum of the individual responses is comparable in magnitude to the ALL response, but the individual responses are delayed with respect to that in ALL. In summary, these results suggest that both ozone-induced stratospheric cooling and tropospheric forcing associated with the SST anomalies contributed to the record tropospheric climate anomalies observed in spring 2011.

1. Introduction

Stratospheric ozone depletion inside polar vortices leads to polar cooling and strengthening of the equator-to-pole temperature gradient. Stronger equator-to-pole temperature gradient induces westerly thermal wind which, in winter, results in a stronger polar night jet [e.g., *Kodera and Yamazaki*, 1994]. Several earlier studies suggested that such stratospheric response may lead to a dynamical response in the troposphere projecting on a positive phase of the annular modes of atmospheric circulation in the corresponding hemisphere [*Thompson and Wallace*, 2000], namely, decreasing/increasing sea level pressure in the polar/middle latitudes, and a poleward shift of the tropospheric westerly winds [*Graf et al*., 1998; *Volodin and Galin*, 1998; *Hartmann et al*., 2000; *Shindell et al*., 1999, 2001]. In the Southern Hemisphere such a response to the ozone depletion during the late twentieth century has been observed in spring-summer [*Thompson and Solomon*, 2002] and simulated by climate models with prescribed or interactive ozone trends [*Sexton*, 2001; *Kindem and Christiansen*, 2001; *Gillett and Thompson*, 2003; *Arblaster and Meehl*, 2006; *Karpechko et al*., 2008; *Perlwitz et al*., 2008; *Son et al*., 2008; *McLandress et al*., 2011], providing a solid evidence of the importance of stratospheric ozone changes for tropospheric climate.

Ozone depletion was also observed in the Arctic in winter and spring during the last decades of the twentieth century although being much less severe than in the Antarctic [*World Meteorological Organization* (*WMO*), 2003; *Solomon et al*., 2007]. It occurred together with a strengthening of the stratospheric polar night jet and a shift of the tropospheric Northern Annular Mode (NAM) toward a more positive phase [*Hurrell*, 1995; *Kodera and Koide*, 1997]. However, unlike in the Antarctic, model studies usually suggested only weak influence of the observed Arctic ozone depletion on tropospheric circulation [*Graf et al*., 1998; *Shindell et al*., 2001; *Gillett et al*., 2003; *Langematz et al*., 2003]; the only study which found a significant influence was that by *Volodin and Galin* [1998]. Thus, although Arctic ozone changes remain to be a candidate forcing for tropospheric circulation changes [e.g., *Morgenstern et al*., 2010] evidences supporting a significant influence of Arctic ozone loss on tropospheric climate trends are lacking.

While the abundance of total column ozone in the Antarctic ozone hole has, in general, evolved in a manner consistent with the time evolution of ozone depletion substances, levels of Arctic ozone destruction are

highly variable from year to year and largely controlled by dynamical processes [*WMO*, 2007, 2011]. In particular, tropospheric planetary-scale wave driving affects stratospheric polar temperatures [e.g., *Newman et al*., 2001; *Orsolini et al*., 2009; *Hurwitz et al*., 2012; *Shaw and Perlwitz*, 2013] and subsequently the magnitude of Arctic ozone loss [e.g., *Salby and Callaghan*, 2007]. Thus, the large variability of Arctic stratospheric climate makes it difficult to detect any ozone-induced changes on Northern Hemisphere tropospheric climate.

In late winter-spring 2011 record chemical Arctic ozone loss was observed that reached 80% at 18–20 km by late March [*Manney et al*., 2011] and 47% in total column ozone at 80°N by early April [*Adams et al*., 2012]. For the first time in the observational record, ozone destruction over the Arctic was comparable to that in the Antarctic ozone hole [*Manney et al*., 2011]. In addition, large positive values of tropospheric NAM index, about 2 standard deviations above the climatology, were observed in late March and April 2011 following the period of a strong stratospheric polar night jet [*Hu and Xia*, 2013]. The April mean tropospheric NAM index values were unprecedented in the National Centers for Environmental Prediction/National Center for Atmospheric Research reanalysis since 1950 (http://www.cpc.ncep.noaa.gov/products/precip/CWlink/daily_ao_index/ao.shtml). These Northern Hemisphere tropospheric circulation anomalies during spring 2011 showed qualitative agreements with tropospheric climate change impacts that have been observed in the Southern Hemisphere as a consequence of stratospheric ozone depletion, raising the question on the influence of the record 2011 Arctic ozone loss on the tropospheric extreme springtime climate event.

It may also be possible that stratospheric ozone forcing, while weak in isolation, can reinforce or suppress impacts of other potential factors. Changes in sea surface temperatures (SSTs) are known to influence the atmospheric circulation both in the troposphere and stratosphere [*Trenberth et al*., 1998; *Hoerling et al*., 2001; *Manzini et al*., 2006; *Deser and Phillips*, 2009]. In particular, *Hurwitz et al*. [2011, 2012] related strengthening of the polar night jet and associated polar stratospheric cooling in late winter 2011, which provided conditions for the chemical ozone loss, to the warm SST anomaly in the subpolar Pacific. Due to large inertia of the ocean, SSTs can be considered an external forcing of the atmospheric circulation and this assumption is often used in attribution studies of decadal atmospheric changes or specific events [e.g., *Deser and Phillips*, 2009; *Perlwitz et al*., 2009]. On the other hand, the atmosphere also contributes to SST changes. In particular, the North Pacific SST anomalies can be partly a response to atmospheric anomalies driven by the El Nino–Southern Oscillation (ENSO) variability [*Alexander et al*., 2002]. Therefore, a caution is needed in interpreting the results of such experiments as proving causality.

The goal of this study is to assess the influence of observed stratospheric ozone anomalies and lower boundary conditions on the spring 2011 tropospheric circulation utilizing experiments with an atmospheric circulation model (AGCM). We show that in our simulations the ozone anomalies of 2011 in isolation do not have a significant impact on the tropospheric circulation. However, we find that the ozone forcing acts as an important amplifier of the effects caused by lower boundary conditions so that the simulated response to the combined ozone and SST influence is in a closer agreement with observations than the responses to each forcing in separation. Our model experiments are described in section 2. The results are reported in section 3 where we first document stratospheric changes (section 3.1) and then tropospheric changes (section 3.2). In section 3.3 we provide a comparison with observations focusing on the response of large-scale circulation as described by the NAM index. Conclusions are presented in section 4.

2. Model Experiments

Numerical experiments are performed with the European Centre/Hamburg version 5 (ECHAM5) AGCM described by *Roeckner et al*. [2006]. The stratospheric version of ECHAM5 used in this study is described by *Manzini et al*. [2006]. The model is used at T63 horizontal truncation and with 47 vertical layers of which the uppermost layer is centered at 0.01 hPa. The responses to specified forcings (ozone and/or SST) are studied by contrasting the control simulation (CONTR) with the forced simulations described below. As in all atmosphere-only experiments with prescribed chemicals and/or ocean boundary conditions, the lack of coupling is somewhat compensated by the use of anomalies of observed magnitude, which is not guaranteed by the interactive models. The use of realistic ozone forcing is especially important here; therefore, we consider the design of our experiments appropriate for our goals.

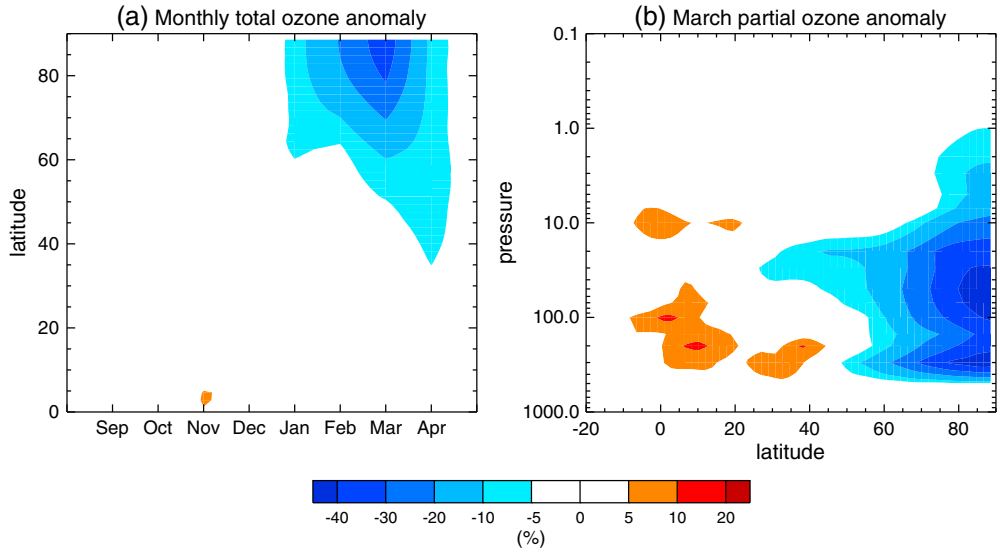

Figure 1. (a) Monthly total ozone anomalies and (b) March mean partial ozone anomaly (%) used in the R-O3 and R-ALL experiments.

Our experiment follows, in general, the approach used for the attribution of climate-related extreme events [e.g., *Perlwitz et al*., 2009; *Stott et al*., 2013]. CONTR is run with the standard ECHAM5 settings representing climate with the CO_2 mixing ratio of 348 ppm. Repeating seasonal cycle in SST and sea ice concentration (SIC) is prescribed using their climatological (1979–2000) monthly mean values from the AMIP2 data set. Monthly mean zonal mean ozone climatology by *Fortuin and Kelder* [1998] is used, which is based on the observations from the period 1980 to 1991. CONTR is run for 52 years, of which the first 2 years are considered spin-up and discarded. Thereafter, three forced experiments are performed; each consisted of an ensemble of fifty 8 month simulations. The simulations start at 1 September of each model year and run until 30 April of the following year. These experiments are as follows:

1. R-O3 is similar to CONTR, except that it is forced by ozone anomalies based on observations from the period from September 2010 to April 2011. Ozone anomalies for this period are taken from the Modern-Era Retrospective Analysis for Research and Applications (MERRA) reanalysis based on the Goddard Earth Observing System (GEOS-5) global atmospheric model [*Rienecker et al*., 2011]. GEOS-5 has ozone as a prognostic field constrained by assimilated observations from Solar Backscatter Ultraviolet. We have verified that the magnitude of the Arctic ozone depletion, which is in the focus of our study, is similar between MERRA and Microwave Limb Sounder (MLS) instrument which has a good coverage in the Polar Regions [*Waters et al*., 2006] (see supporting information). The benefit of using MERRA is that it provides continuous time series, thus facilitating construction of the boundary conditions. This is not the case with MLS which have breaks during the considered period. The monthly zonal mean ozone anomalies 2010/2011 are calculated with respect to the monthly MERRA climatology 1980–1991 and then added to the monthly zonal mean ozone climatology used in CONTR, assuming that the atmospheric response only depends on the ozone anomaly and not sensitive to the underlying ozone climatology. During austral spring the anomaly field includes a strong signature of the Antarctic ozone hole. We have chosen to restrict the focus to the Northern Hemisphere ozone anomalies and removed the Southern Hemisphere anomalies by applying a filter with weights equal to zero south of 20°S, equal to one north of the equator, and smoothly increasing from zero to one between 20°S and the equator. Monthly total ozone anomalies are shown in Figure 1a. The anomaly field is dominated by the polar depletion in late winter-spring which peaks in March. Vertical cross section of partial ozone anomaly for March 2011 is shown in Figure 1b. Note that only a part of the prescribed ozone anomaly results from the chemical loss. The other part is the result of the specific transport conditions that occurred in 2011. Since Arctic ozone loss always occurs in conjunction with reduced poleward transport, we are not interested in studying the response to chemical loss separately. Reduced poleward transport is accompanied by a

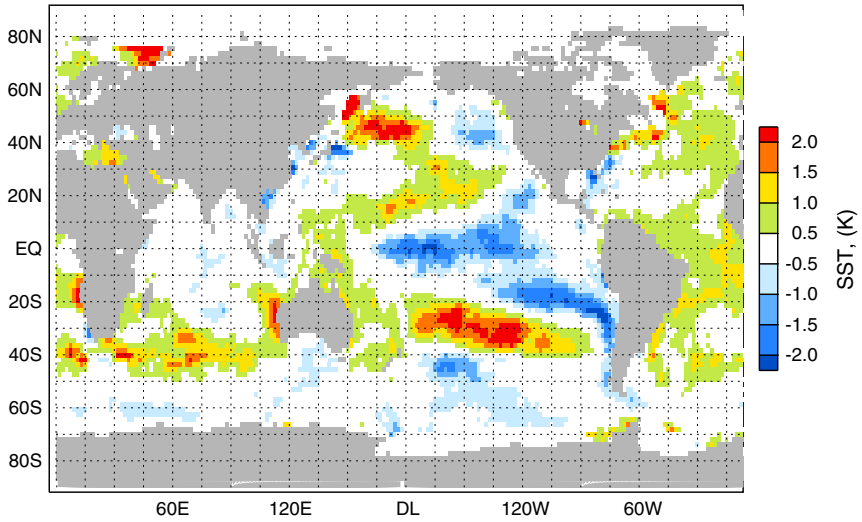

Figure 2. January–March mean SST anomalies in 2011 with respect to the period 1979–2010 used in the R-SST and R-ALL experiments.

slower upwelling in the Tropics which results in positive ozone anomalies there (Figure 1). It should be kept in mind that the prescribed ozone anomalies maximize in mid-March by model construction, whereas in spring 2011 they maximized in late March, about 2 weeks later when there is more sunlight and the ozone anomaly is of more importance. This mismatch of timing likely reduces the simulated response to ozone forcing. However, we note that recent simulations with another model [*Smith and Polvani*, 2014] show insignificant tropospheric circulation response to ozone anomalies even larger than those used here, which is consistent with the results of the R-O3 experiment reported below. Thus, we expect that the mismatch does not qualitatively affect our results but may influence the timing of the tropospheric response.

2. The R-SST experiment is similar to CONTR, except that the global SST and SIC anomalies corresponding to the period September 2010 to April 2011 have been used. The anomalies are calculated from the Hadley Centre Sea Ice and Sea Surface Temperature (HadISST) data set [*Rayner et al*., 2003], with respect to the HadISST 1979–2010 climatology and then added to the Atmospheric Model Intercomparison Project 2 (AMIP-2) climatology used in CONTR. We do not expect our results to be sensitive to our choice of SST data set: differences between HadISST and AMIP-2 are significant only in limited areas [*Hurrell et al*., 2008].

   Figure 2 shows the observed mean SST anomalies for January–March. In winter/spring 2011 the lower boundary conditions were characterized by La Niña like conditions as seen from the negative temperature anomalies in the tropical Pacific. The positive SST anomalies in the North Pacific, which *Hurwitz et al*. [2011, 2012] linked to unusually weak tropospheric wave driving and strong Arctic vortex in late winter 2011, are also apparent. Note that the positive anomalies in the North Pacific region in our experiments are about 30% smaller than those used in *Hurwitz et al*. [2012] who calculated their anomaly as a difference between years with warm North Pacific SST (1991 and 1997) and cold SST (1987 and 1988) rather than directly using the 2011 conditions, as is done here. The globally average January–March SST anomaly in our experiment is 0.2 K. This may be related to a climate change signal, which is a part of the lower boundary conditions. This signal is, however, much smaller than the regional anomalies due to interannual variability.
3. The R-ALL experiment includes the ozone fields from the R-O3 experiment and the SST/SIC fields from the R-SST experiment.

For comparison with model simulations, we utilize 500 hPa geopotential heights, zonal winds, and air temperatures from European Centre for Medium-Range Weather Forecasts ERA-Interim reanalysis [*Dee et al*., 2011].

Statistical significance of the differences between experiments are tested using two-sample, two-tailed *t* test with $p = 0.05$, where p is the probability to wrongly reject the null hypothesis. To test whether the

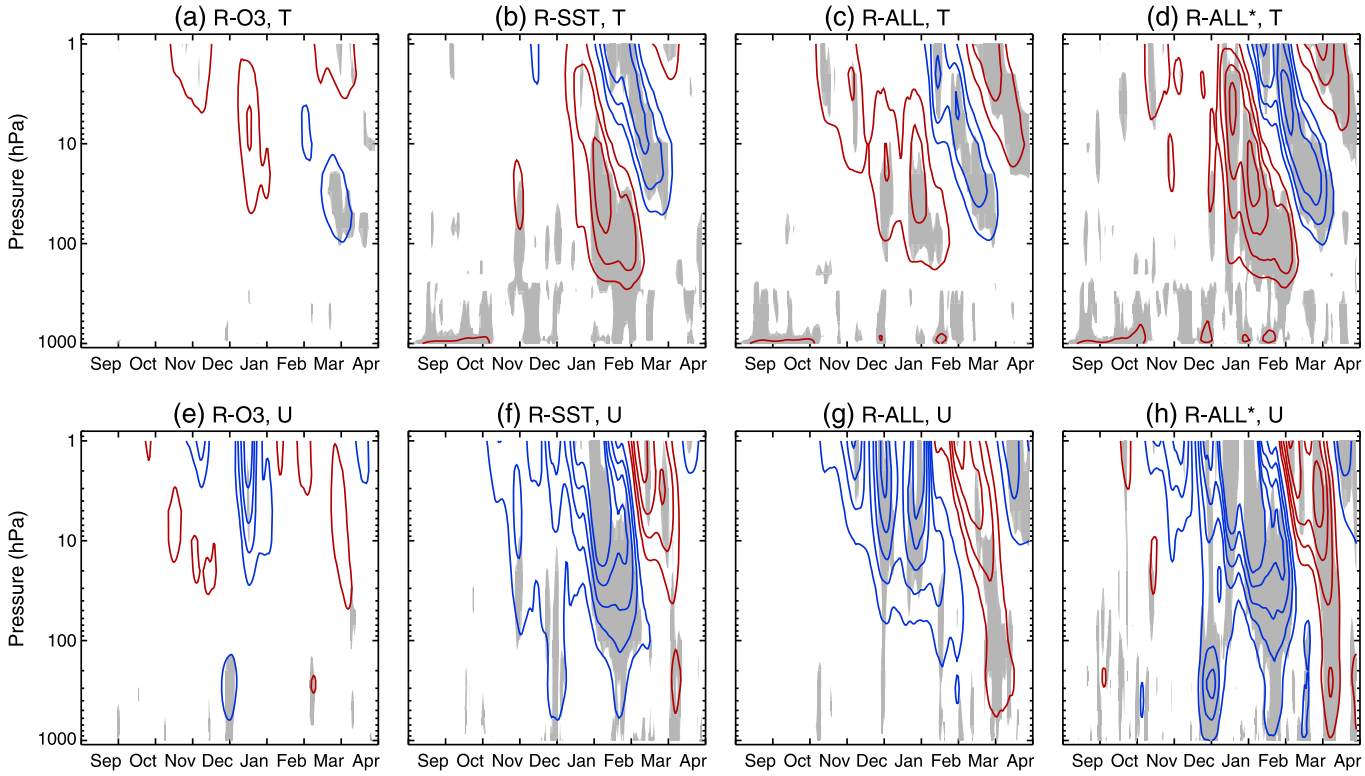

Figure 3. (a–d) Daily mean polar (70–90°N) temperature responses and (e–h) daily mean zonal winds (55–65°N) responses in R-O3, R-SST, R-ALL, and R-ALL*. The anomalies are smoothed with a 11 day moving average. Shading indicates statistically significant responses ($p < 0.05$). Red (blue) contours mark positive (negative) responses. Contours are drawn at ±1.5, 3, and then each 1.5 (K for temperature and m/s for zonal winds).

responses to ozone and SST are additive we use outputs of CONTR, R-O3, and R-SST experiments to construct synthetic ensemble R-ALL* as follows:

$$\text{R ALL*} = \text{CONTR} + (\text{R O3} - \text{CONTR}) + (\text{R SST} - \text{CONTR}) = \text{R O3} + \text{R SST} - \text{CONTR}$$

Thereafter, the variance of R-ALL* is reduced by factor 3 to account for the increase of the variance due to summing of the three time series. (Here the assumption of equality of the variances is used.) In practice, it is done by dividing the R-ALL* anomalies (i.e., deviations from the respective R-ALL* means) by squared root of 3. Then, the standard two sample *t* test is applied to the difference between R-ALL and R-ALL*. The synthetic time series are only used to test the additivity of the mean responses but not to study other changes in variable distributions.

3. Results

3.1. Stratospheric Response

Figure 3 shows daily polar temperature (70°N–90°N) and daily zonal mean zonal winds (55°N–65°N) responses (i.e., differences between the forced experiments and CONTR) for the R-O3, R-SST, R-ALL, and R-ALL* experiments. There are periods of significant responses starting already in autumn, for example, in the troposphere in R-SST and R-ALL resulting from the prescribed SST and SIC anomalies. In this study we focus on the period of ozone depletion, i.e., late winter to early spring.

In R-O3 (Figure 3a), there is a cooling response with a maximum of about 2 K between 20 and 70 hPa at the end of March. In April the maximum cooling shifts downward and weakens. In R-SST (Figure 3b), there is also a cooling in February–March which is coincident with the period of ozone depletion although no ozone depletion is prescribed in this experiment. While in the R-O3 run, the cooling is confined to the lower stratosphere, consistent with the radiative forcing incorporated there, the cooling in R-SST starts at higher altitude with anomalies exceeding 5 K above 10 hPa. In the R-SST run the cooling propagates downward up

Table 1. Statistics of Polar (70°N−90°N) 50 hPa Air Temperature Response in March and 100 hPa Eddy Heat Flux Averaged Between 45°N and 75°N and From 1 February to 20 March[a]

	T, 50 hPa, March			Heat Flux, 100 hPa, February–March				
	Mean K	$<-1\sigma$ years	$>1\sigma$ years	Mean (m s^{-1} K)	$<-1\sigma$ years	$>1\sigma$ years	Correlation Coefficients Between *T* and Heat flux	Slope of *T* Regression on Heat Flux K (m s^{-1} K) ^{1}
CONTR	-	9	10	14.98	8	10	**0.69** (**0.001**)	**1.03** (**0.001**)
R-O3	−1.14 (0.19)	15	5	14.50 (0.37)	10	6	**0.87** (**0.001**)	**1.52** (**0.001**)
R-SST	−0.10 (0.90)	10	9	14.39 (0.27)	11	7	**0.67** (**0.001**)	**1.06** (**0.001**)
R-ALL	**−1.79 (0.03)**	18	5	**13.76 (0.03)**	14	3	**0.72 (0.001)**	**1.08 (0.001)**
R-ALL*	−1.25 (0.13)	-	-	13.91 (0.06)	-	-	-	-

[a]Shown are the mean values and the numbers of years when the corresponding ±1 standard deviation anomaly of CONTR experiment is exceeded. Also shown are the correlation coefficients between temperatures and heat flux and the slope of temperature regression on the heat flux. Numbers in parentheses indicate significance levels. Significant responses ($p < 0.05$) are marked in bold.

to 50 hPa consistent with wave-mean flow interactions. *Hurwitz et al*. [2012] found a cooling stratospheric response in a model experiment with prescribed warm SST anomaly in the subpolar North Pacific, broadly similar to that observed in 2011 and prescribed in the R-SST experiment (Figure 2). Interestingly, the significant warming in January–February in R-SST is not simulated by *Hurwitz et al*. [2012], suggesting that it is likely related to SST anomalies from regions other than the North Pacific. *Omrani et al*. [2014] showed that warming in the North Atlantic (see Figure 2) is associated with weakened polar stratospheric vortex in early to midwinter, which is qualitatively consistent with our results.

In R-ALL (Figure 3c), the cooling response in March extends down to 100 hPa, similar to R-O3, but with a larger magnitude. In the upper stratosphere the magnitude of the cooling response in R-ALL is comparable to that in R-SST. Table 1 provides additional information about the response of the lower stratospheric temperatures in March. R-ALL is the only experiment with significant ($p < 0.05$) monthly mean cooling response at 50 hPa, although its magnitude is rather weak (−1.8 K). When averaged over the 2 month March–April period both R-ALL and R-O3 show a significant cooling of −1.2 K at 50 hPa, but the cooling in R-SST is not significant (not shown). Table 1 also shows the number of simulated cold and warm March values defined as months with a mean anomaly exceeding 1 standard deviation of the CONTR experiment. As seen in Table 1, the number of simulated cold/warm March values is increased/decreased in R-O3 and R-ALL compared to CONTR. Thus, the whole probability distribution functions (PDF) in R-O3 and R-ALL, but not in R-SST, are shifted toward colder values.

The responses of the stratospheric winds (Figures 3e–3g) are coupled to those of the polar temperature via thermal wind relation. All three experiments reveal a strengthening of the westerly winds in the lower stratosphere in March and April in agreement with the polar stratospheric cooling, but the R-O3 response is weak and only significant for a short period of time (Figure 3e). In R-ALL, the strengthening propagates down to the troposphere by mid-March. The tropospheric wind response is less pronounced in R-SST and almost indiscernible in R-O3.

Figure 3 also shows the response of the synthetic simulations R-ALL* which represents the sum of individual responses to the ozone and SST anomalies (see section 2). In R-ALL*, the warming response in the stratosphere in midwinter associated with SST forcing is more pronounced and lasts until mid-March, so that the cooling response is delayed compared to that in R-ALL. Monthly mean cooling in March is not significant (Table 1), but it becomes significant when averaged over March–April. Consistent with the temperature response, the response of the lower stratospheric wind is significantly negative until March, while the positive response associated with the combined ozone and SST forcing is delayed compared to R-ALL. Also in the troposphere, a negative wind response, mainly associated with SST forcing, is seen until mid-March, while the positive response, which is comparable in magnitude to that in R-ALL, is only seen in April.

The dynamical variability of wintertime Arctic stratosphere is driven by planetary waves propagating from the troposphere. These waves are sensitive to both the strength of the tropospheric sources and transmitting properties of the stratospheric basic state. In order to better understand the zonal mean responses seen in Figure 3, we next assess changes in the tropospheric wave forcing of the stratosphere. Table 1 shows the relation between lower stratospheric temperatures in March and eddy heat flux at 100 hPa averaged over

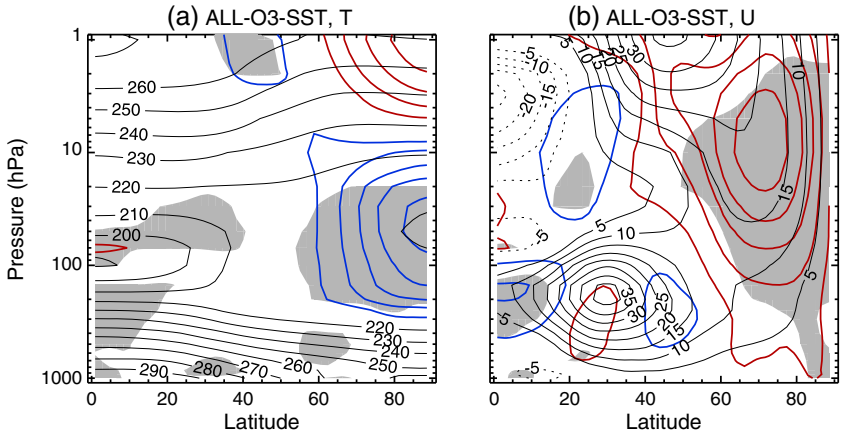

Figure 4. The difference between zonal mean (a) temperature and (b) zonal wind responses in R-ALL and R-ALL* averaged between 1 February and 20 March. Shading indicates statistically significant differences ($p < 0.05$). Red (blue) contours mark positive (negative) differences. Contours are drawn at ±0.5, 1.0, and then each 0.5 K for temperature and at ±0.5, 1.5, and then each 1 m/s for zonal winds. Gray contours mark CONTR climatology.

45°N–75°N and from 1 February to 20 March. The period of heat flux averaging is chosen to maximize the correlation with March temperatures. The lead time of the eddy heat flux is consistent with the understanding that lower stratospheric temperatures are primarily controlled by the eddy heat flux accumulated during the preceding 1–2 months [*Newman et al.*, 2001]. The overlap between the averaging periods implies that two-way interactions between eddy heat flux and temperatures contribute to the correlation.

Table 1 shows that, in all experiments, March temperatures are closely related to the eddy heat flux with correlation coefficients for different experiments ranging between 0.67 and 0.87. The slopes of the linear regression fits are roughly similar between the experiments. As seen from Table 1, eddy heat flux distributions in the three forcing experiments are shifted toward lower values compared to CONTR, although only in R-ALL is the mean eddy heat flux response significant at $p < 0.05$. In R-O3 the reduction of heat flux is apparently associated with reduced wave propagation to the polar stratosphere due to ozone-induced radiative cooling. In R-SST, it is likely related to a reduced tropospheric wave activity associated with prescribed SST anomalies. In R-ALL, the reduction is largest and is likely due to the combination of both factors. From the slope of the temperature regression on the heat flux, it can be inferred that the reduction of heat flux can explain a large portion of the March cooling response in the experiments.

A more detailed analysis of the temperature/heat flux relation reveals that temperature difference between the experiments with climatological ozone (CONTR and R-SST) and those with prescribed ozone depletion (R-O3 and R-ALL) is larger toward the smaller heat flux values. The mean temperature anomalies for winters with anomalously weak eddy heat flux (i.e., with heat flux less than 1 standard deviation anomaly in the CONTR experiment) are -3.1 ± 3.7 K and -3.9 ± 3.3 K in CONTR and R-SST, respectively, and -7.8 ± 2.1 K and -5.7 ± 2.1 K in R-O3 and R-ALL, respectively. The temperature difference between these two groups (i.e., CONTR and R-SST on the one hand and R-O3 and R-ALL on the other hand) is statistically significant at $p = 0.001$. This difference cannot be explained by a difference in the eddy heat flux because, for these two subsets of data, the heat flux difference is 0.3 K m s^{-1} only. Thus, the difference most likely arises due to the direct impact of ozone-induced radiative cooling on temperatures. There is no corresponding difference between these experiments for winters with anomalously large heat flux (>1 standard deviation anomaly in the CONTR experiment). During these winter the mean temperatures anomalies are 4.8 ± 1.8 K and 4.5 ± 2.5 K in CONTR and R-SST, respectively, and 5.8 ± 2.3 K and 3.4 ± 3.2 K in R-O3 and R-ALL, respectively. This suggests that the direct radiative impact of ozone on temperatures is mainly discernible during dynamically inactive winters.

The major influence of strongly nonlinear wave-mean flow interactions on the atmospheric responses to ozone and SST anomalies, corroborated by the analysis of Figure 3, raises the question of whether the ozone and SST responses are additive. Figure 4 shows the zonal mean temperature and zonal wind differences between R-ALL and the synthetic R-ALL* simulation averaged between 1 February and 20 March.

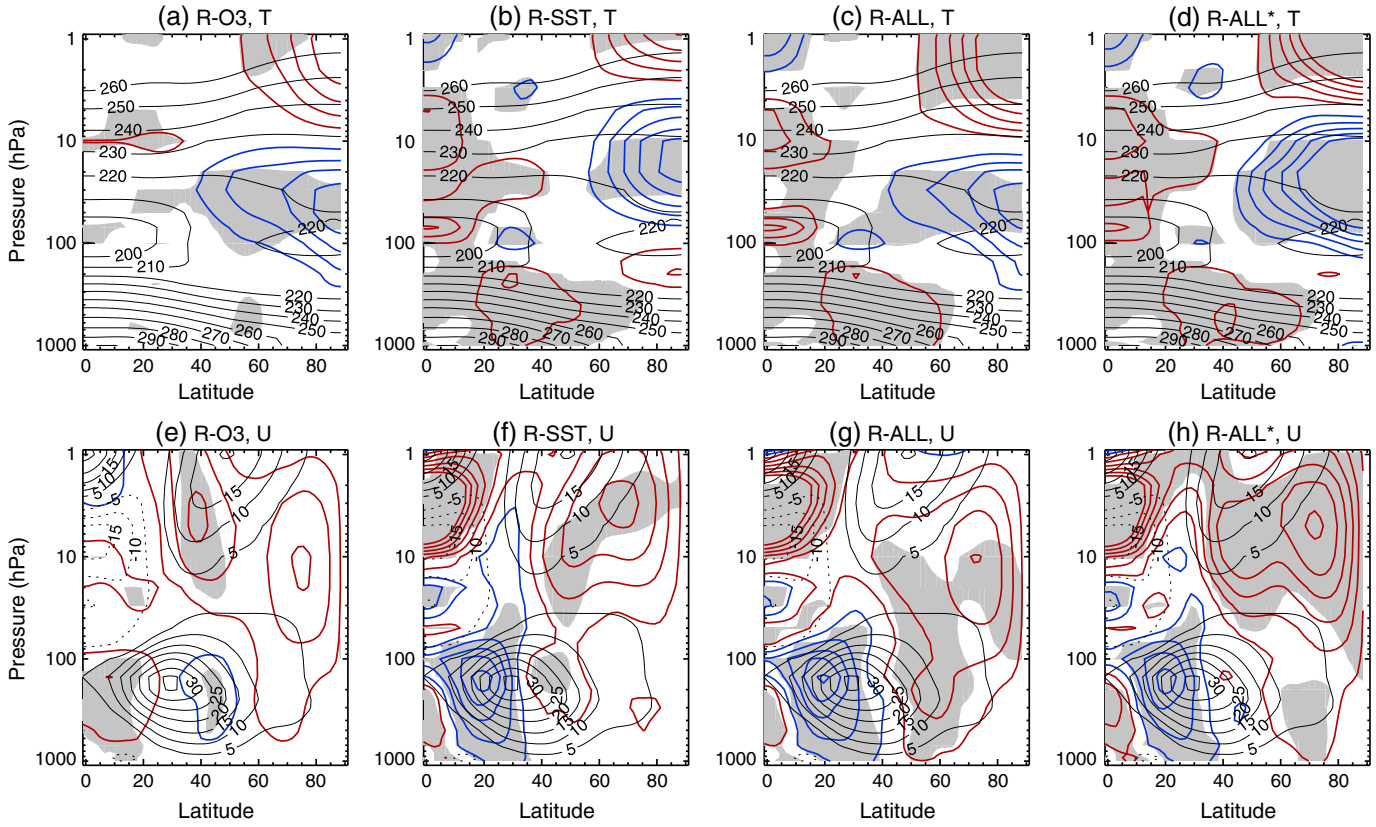

Figure 5. Zonal mean (a–d) temperature and (e–h) zonal wind responses averaged between 17 March and 15 April. Shading indicates statistically significant differences from CONTR ($p < 0.05$). Red (blue) contours mark positive (negative) differences. Contours are drawn at ±0.5, 1.0, and then each 0.5 K for temperature and at ±0.5, 1.5, and then each 1 m/s for zonal winds. Gray contours mark CONTR climatology.

(The result is not sensitive to changes in the period of averaging, i.e., similar result is obtained if the averaging is done over February.) Figure 4 shows that, during this period, which is characterized by an average warming response in both R-ALL and R-ALL* (Figure 3), the polar lower stratospheric temperature response is significantly lower (i.e., less positive) and the stratospheric winds response is significantly more positive (i.e., less negative) in R-ALL than in R-ALL*. Temperature differences exceed 2 K in the polar lower stratosphere, which is comparable to the magnitude of the responses themselves. This suggests that the stratospheric R-ALL response cannot be understood as a linear superposition of individual responses to ozone and SST anomalies and that nonlinear effects due to the interactions between planetary waves and the mean flow play a significant role in the R-ALL response.

Overall, our experiments suggest that Arctic stratospheric ozone anomalies even as large as those occurred in 2011 can induce only a modest dynamical response if considered alone. The variability of the Arctic stratosphere is dominated by internal variability with a nonnegligible contribution from the forced component associated with SST anomalies, in agreement with previous studies. Our experiments also reveal that the ozone forcing has modified the impact of 2011 SST conditions so that the response to their combined forcing is significantly different from the sum of their individual responses.

3.2. Tropospheric Response

In this section we consider the impacts of the stratospheric anomalies on the tropospheric circulation in more detail. We focus on the period between mid-March and mid-April (17 March to 15 April) because this is the period of the maximum tropospheric wind response. Similar results are obtained if the considered period is extended from mid-March to the end of April, unless otherwise mentioned.

Figure 5 shows zonal mean temperature and zonal wind responses for this period in the three experiments and R-ALL*. It is seen that the tropospheric circulation responses in R-SST and R-ALL involve the poleward

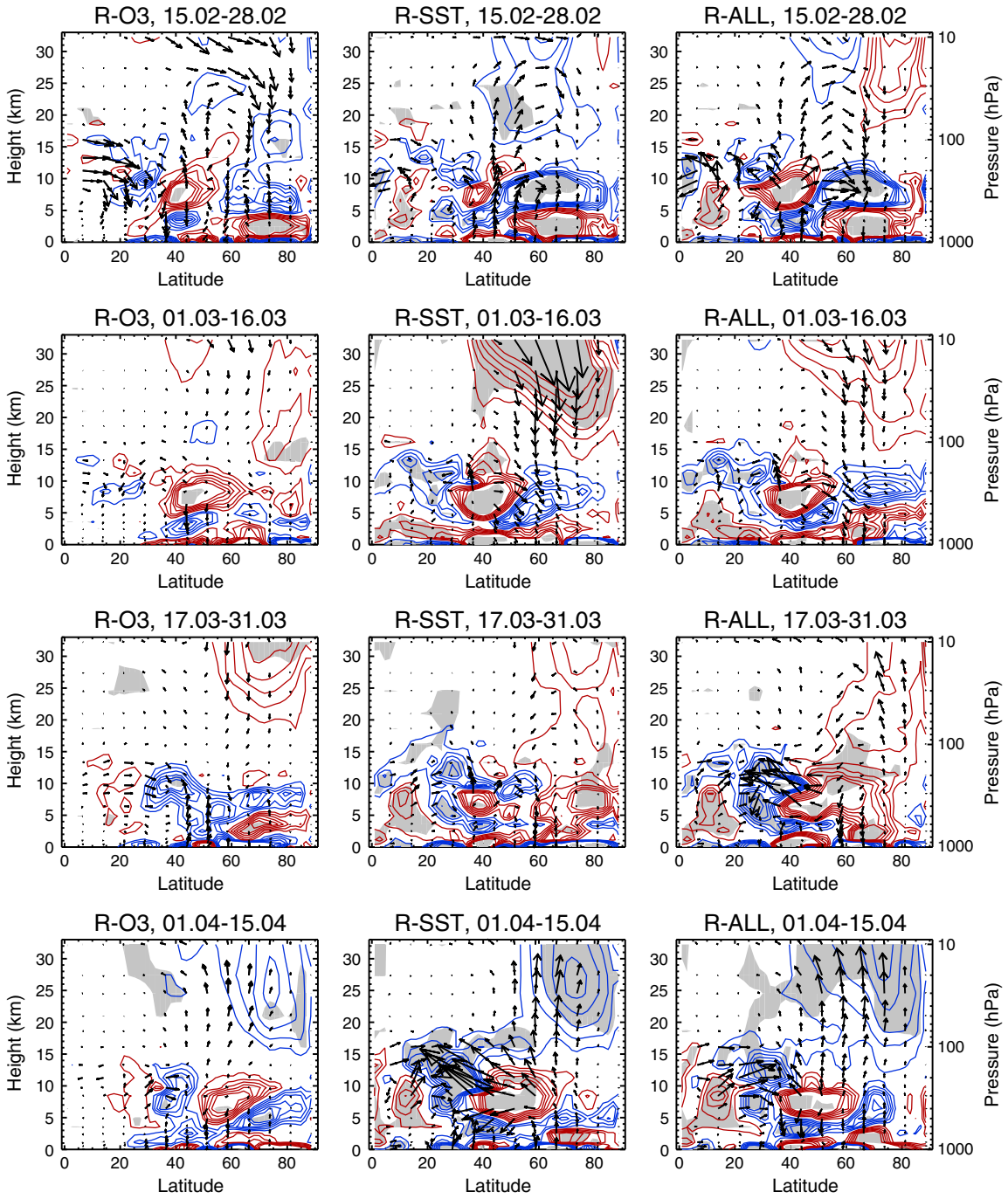

Figure 6. Responses of EP flux vectors (arrows) and EP flux divergence (contours, m/s/d) averaged for half-month periods between 15 February and 15 April. Shading indicates statistically significant responses of the EP flux divergence ($p < 0.05$). Red (blue) contours mark positive (negative) differences. Contours are drawn at ±0.5, 1.5, and then each 1 m/s/d.

shift of the extratropical winds consistent with a shift toward more positive NAM index values, although in R-SST this response does not extend to the surface. In R-O3 the tropospheric wind response is not significant and does not clearly project on the positive NAM phase.

The response of the tropospheric winds in R-ALL* is similar in sign but weaker than that in R-ALL. However, this difference is sensitive to the period of averaging and is negligible if averaging is extended to the end of April. As can be seen in Figure 3, strengthening of the tropospheric winds is delayed in R-ALL*

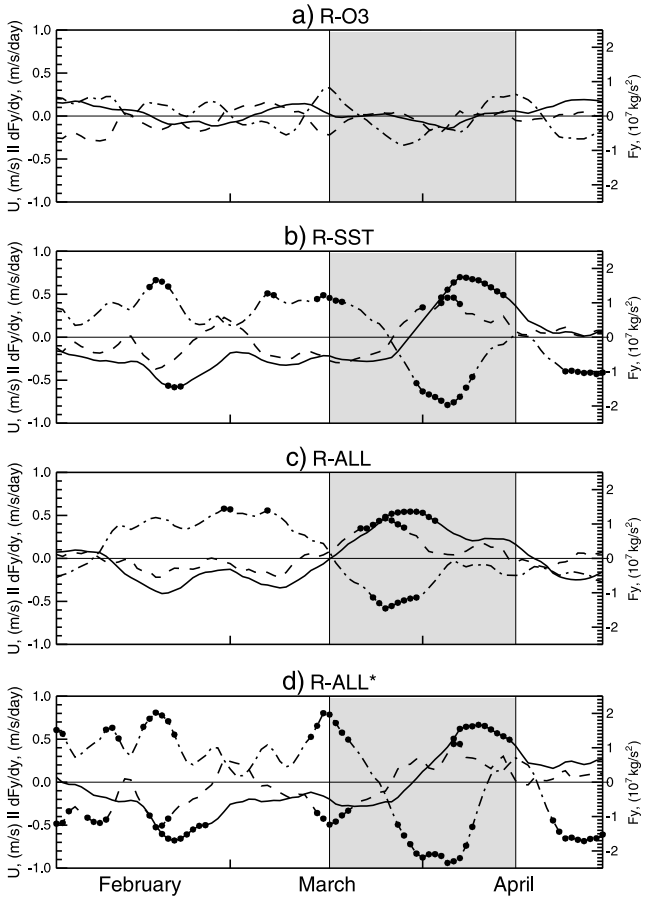

Figure 7. Zonal winds (m/s) at 1000 hPa averaged over 45°N–60°N (solid); meridional component of EP flux, Fy (kg/s^2), at 300 hPa averaged north of 40°N (dash-dotted); meridional divergence of Fy (m/s/d) averaged over 45°N–60°N and between 700 hPa and 100 hPa (dashed). The anomalies are smoothed with an 11 day moving average. Solid circles indicate statistically significant responses ($p < 0.05$). Shaded is the period of averaging in Figure 5.

compared to R-ALL, associated with both a significantly stronger stratospheric warming in February and early March and a delayed stratospheric cooling in R-ALL*.

Numerous studies have demonstrated that the response of the tropospheric circulation to stratospheric anomalies is driven by the interactions between tropospheric waves and zonal mean flow [*Kuroda and Kodera*, 1999; *Limpasuvan et al.*, 2005; *Chen and Zurita-Gotor*, 2008; *Kuroda*, 2008]. *Limpasuvan et al.* [2005] demonstrated, using reanalysis data, that polar stratospheric vortex intensification events are usually followed by a distinct reorganization of tropospheric waves. This includes an anomalous equatorward Eliassen-Palm (EP) flux in the upper troposphere and a dipole of anomalous EP flux divergence in the free troposphere with a positive/negative lobe in midlatitudes/subtropics. The pattern of the tropospheric response is consistent with positive NAM phase identified earlier in reanalysis by *Limpasuvan and Hartmann* [2000]. Here we analyze the simulated eddy response in order to demonstrate that, in our experiments, the response is consistent with changes seen in a composite of observed stratosphere-troposphere coupling events analyzed by *Limpasuvan et al.* [2005], i.e., the same mechanisms are likely causing the response in the model as in observations.

Figure 6 shows Eliassen-Palm (EP) fluxes and their divergence for the sequence of half-month (~15 day) periods between 15 February and 15 April. In all experiments the end of February is marked by an equatorward shift of the region of upward planetary wave propagation resulting in a less upward propagation to the polar stratosphere north of 60°N. In March the reduced upward propagation leads to anomalous EP flux divergence in the polar stratosphere in all experiments, most noticeably in R-SST during the first half of March. This anomalous EP flux divergence drives the stratospheric wind strengthening seen in Figure 3. In R-O3, the EP -flux anomalies during March and April are in general smaller than in the other two experiments, consistent with the weak zonal wind response seen in Figures 3 and 5.

Figure 6 shows that the anomalous equatorward EP flux in the upper troposphere is simulated in R-SST and R-ALL following the stratospheric anomalies. In R-SST it is simulated during the first half of April, while in R-ALL it is simulated starting from mid-March, i.e., for a longer period compared to R-SST. This can be more clearly seen in Figure 7 which shows the time series of the meridional EP flux at 300 hPa averaged north of 40°N (see also Table 2). Thus, in R-SST and R-ALL the changes in the tropospheric waves are consistent with the response to stratospheric vortex intensification identified in a composite of observed events by *Limpasuvan et al.* [2005]. In R-O3, the response averaged between mid-March and mid-April is weak as seen in Figure 7 and Table 2. In R-ALL*, the response is close to that in R-SST (see Figure 7 and Table 2).

Table 2. Responses of 1000 hPa Zonal Winds (U) Averaged Over 45°N–60°N; Meridional Component of EP Flux (Fy) at 300 hPa Averaged North of 40°N, and Meridional Divergence of Fy (dFy/dy) Averaged Over 45°N–60°N and Between 700 hPa and 100 hPa[a]

	Eddies and 1000 hPa Winds, March–April			NAM (500 hPa), March–April		
	U 1000 hPa m/s	dFy/dy (m/s/d)	Fy 10^6 kg/s^2	Mean	$<-1\sigma$ years	$>1\sigma$ years
CONTR	-	-		-	8	9
R-O3	−0.02 (0.90)	−0.02 (0.88)	−0.9 (0.88)	0.04 (0.85)	10	11
R-SST	0.17 (0.31)	0.11 (0.35)	−4.3 (0.26)	0.17 (0.38)	3	8
R-ALL	**0.33 (0.05)**	**0.23 (0.04)**	−6.6 (0.07)	**0.45 (0.03)**	5	15
R-ALL*	0.14 (0.38)	0.09 (0.46)	−5.2 (0.16)	0.21 (0.30)	-	-

[a]Also shown are statistics of 500 hPa NAM index. All quantities are shown for the period 17 March to 15 April. Numbers in parentheses indicate significance levels. Significant responses ($p < 0.05$) are marked in bold.

A pattern of positive EP flux divergence responses north of about 40°N and negative EP flux divergence response south of 40°N in the free troposphere (between 5 and 10 km) can also be seen in R-O3 and R-SST in April, while in R-ALL such a response is simulated starting from mid-March (Figure 6). The positive EP flux divergence drives strengthening of the zonal winds. In the upper troposphere the EP flux divergence is mainly associated with the divergence of the meridional component of the EP flux, which is proportional to the convergence of eddy momentum flux. Vertically averaged convergence of eddy momentum flux is balanced by the surface friction associated with surface wind. Figure 7 shows the time evolution of the vertically averaged convergence of the eddy momentum flux along with the near-surface winds north of 45°N. A strengthening of the midlatitude near-surface winds, which is an integral part of the positive NAM phase, is seen in R-ALL from mid-March to mid-April and in R-SST during the first half of April. These strengthening periods coincide with the anomalous equatorward EP-flux and the convergence of the eddy momentum fluxes. Thus, the above analysis reveals that, in our simulations, changes in the tropospheric eddies are consistent with the response to stratospheric vortex intensification identified previously in the reanalysis data and suggests that the response of the tropospheric winds is driven by changes in the tropospheric eddies.

It has been shown in numerous studies that the tropospheric response to stratospheric anomalies strongly projects on the NAM [e.g., *Baldwin and Dunkerton*, 2001; *Limpasuvan et al*., 2005]. We next analyze the simulated NAM response during the period from mid-March to mid-April. The NAM is defined as the first Empirical Orthogonal Function (EOF) of the December–April daily zonal mean 500 hPa geopotential height anomalies north of 20°N from the CONTR experiment and is shown in Figure 8. Also shown in Figure 8 is the NAM pattern calculated from the ERA-Interim data using daily zonal mean 500 hPa geopotential height anomalies with respect to the 1979–2010 period. Both in the model and in reanalysis, the first EOF exhibits a seesaw pattern of the height field between middle and high latitudes. The correlation between observed and simulated patterns is 0.99, although the simulated anomalies at high latitudes are enhanced compared to reanalysis. The daily NAM index for each winter and for all experiments is calculated as a projection of the daily zonal mean geopotential height anomalies on the NAM pattern. Then, the daily indexes are averaged between 17 March and 15 April. Finally, all indexes are standardized by subtracting the mean and dividing by the standard deviation of the NAM index from the CONTR experiment.

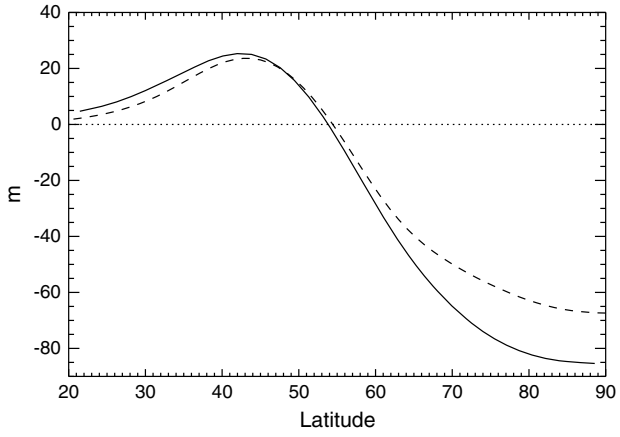

Figure 8. Simulated (solid) and observed (dashed) NAM patterns at 500 hPa based on December–April daily zonal mean geopotential height anomalies (m). Simulated pattern is based on CONTR simulations.

PDFs of the simulated NAM indexes are shown in Figure 9. Only in R-ALL we

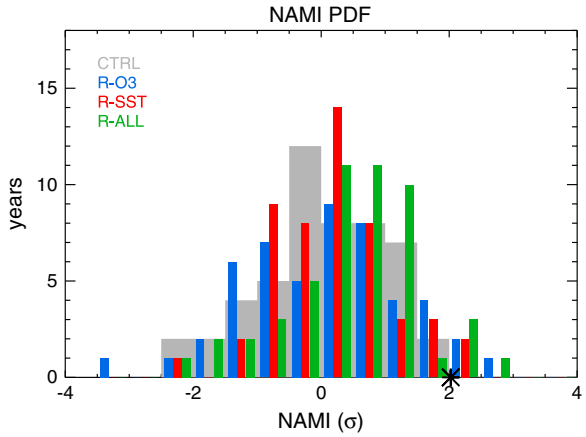

Figure 9. Probability distribution function of 500 hPa NAM index values averaged between 17 March and 15 April determined based on 50 ensemble members for the individual experiments. The star indicates the observed value.

find a significant positive mean NAM index response ($p < 0.05$, see Table 2). The positive NAM response is consistent with the poleward shift of the extratropical tropospheric winds seen in Figure 5. In R-ALL, the frequency of occurrence of a strongly negative/positive NAM index (less/more than $\pm 1\sigma$) is considerably reduced/enhanced compared to that in the CONTR experiment. In the other two experiments the changes in the frequency of large-magnitude NAM events are less pronounced. We also find similar results in the NAM-like pattern response at the 1000 hPa. In R-ALL, the 1000 hPa mean NAM-like pattern response is 0.4σ, comparable to the 500 hPa NAM response but significant at $p = 0.07$ only. The reduced significance of the 1000 hPa response may be attributed to a larger contribution of the local processes, and thus larger noise, near the surface compared to that in the free atmosphere.

We also test for a sensitivity of the results to the period of averaging. We find a significant positive monthly mean NAM response in April in R-SST, R-ALL, and R-ALL*, but not in R-O3. Only in R-ALL does the NAM response remain significant when averaged over the 1.5 month period from mid-March to the end of April suggesting that the combined influence of ozone and SST anomalies in R-ALL may have prolonged the response of the tropospheric circulation compared to the responses to individual forcings.

In summary we have demonstrated that the simulated response of the tropospheric circulation is consistent with the expected response to stratospheric vortex intensification and that this response is the strongest in the R-ALL experiment. In R-ALL, a significant mean NAM response lasts for longer than a month and includes an increased probability of occurrence of positive NAM events of large magnitude.

3.3. Comparison With Reanalysis

Our results shown above illustrate a significant impact of the combined SST-ozone forcing on the tropospheric circulation. Here we provide a comparison of our simulations with observed anomalies in 2011 focusing on the NAM response. The star in Figure 9 indicates the observed mean NAM index for the period 17 March to 15 April 2011 estimated from the ERA-Interim data. Consistent with *Hu and Xia* [2013], we find a strongly positive NAM index value of 2.02σ in the reanalysis in spring 2011. Our simulations suggest that NAM index value exceeding 2σ is a rare event with index value of such magnitude appearing only twice in R-SST, 3 times in R-O3, 4 times in R-ALL, and never in CONTR. In the following we determine the conditions which make the occurrence of such extreme NAM events in the model more likely.

Based on observations, *Black and McDaniel* [2004] showed that, for tropospheric NAM anomalies to emerge from a stratospheric event, stratospheric anomalies are required to descend to sufficiently low altitudes within the stratosphere. Furthermore, the tropospheric response depends on the detailed nature of preexisting NAM in the troposphere. Figure 10 shows the same quantities as Figure 3 but for the four R-ALL ensemble members with the NAM index exceeding 2σ together with the ERA-Interim anomalies in 2010/2011. We note that selection of two to five R-ALL ensemble members with the largest NAM index results in a similar pattern of the responses but with different magnitudes.

Although the magnitude of the simulated responses is, in general, considerably smaller than the observed anomaly, there are striking similarities between the simulated responses and observed anomalies in late winter to spring. In both model and observations, the cooling anomalies start in the upper stratosphere in January and then progress to the lower stratosphere. In observations the downward propagation is more abrupt and the anomaly has a larger vertical extension compared to the model. It is also of interest to

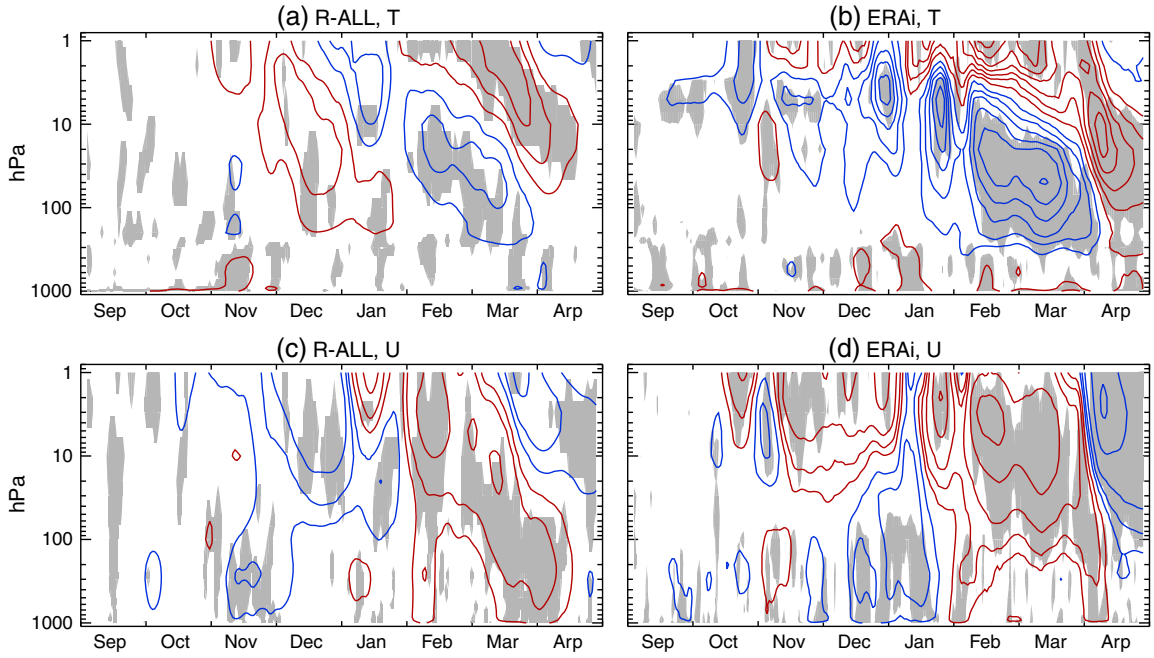

Figure 10. Daily mean (a) polar temperatures (70–90°N) and (c) zonal winds (55–65°N) response averaged over four selected R-ALL simulations. These R-ALL simulations have the largest positive NAM index value at 500 hPa in the period 17 March to 15 April. ERA-Interim daily mean (b) polar (70–90°N) temperature and (d) zonal wind (55–65°N) anomalies in 2010/2011 with respect to 1979–2010. All anomalies are smoothed with an 11 day moving average. Red (blue) contours mark positive (negative) differences. Contours are drawn at ±2, 5, 8, and then each 3 K for temperature and at ±2, 5, 10, and then each 10 m/s for zonal winds. Shading in Figures 10a and 10c indicates an agreement in the sign of the response across all four simulations and in Figures 10b and 10d differences exceeding 1σ of the observed 1979–2010 anomalies.

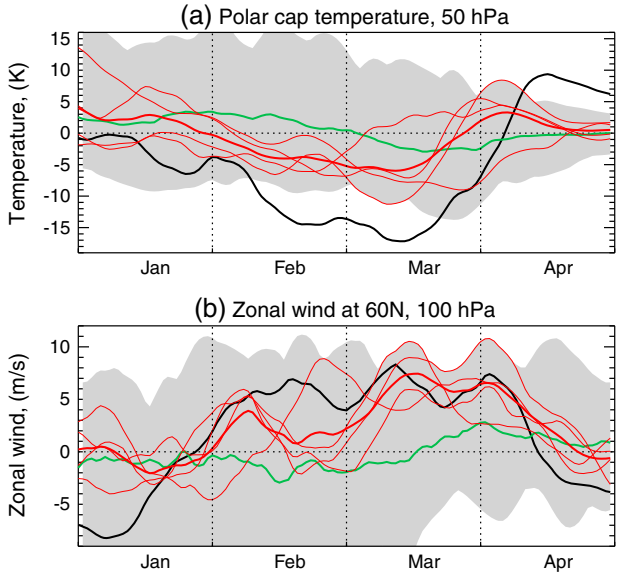

Figure 11. Time series of responses in (a) polar temperatures (70–90°N) at 50 hPa and (b) zonal winds (55–65°N) at 100 hPa for the four selected R-ALL simulations shown in Figure 10 (thin red), their mean (thick red), overall R-ALL mean (green), and ERA-Interim (black). The anomalies are smoothed with an 11 day moving average. Shading indicates the range of responses across all R-ALL simulation.

compare Figure 3c, which shows the average of all R-ALL ensemble members, with Figure 10a. While Figure 3c features a warming response in the lower stratosphere through the most of February, a cooling response is seen in Figure 10a, in agreement with observations. This suggests that the large magnitude of the 2011 event requires a preconditioning which is not a part of the forced signal, because this is not seen in the average across all simulations but rather a result of internal dynamics. A similar conclusion can be drawn based on the zonal wind analysis. Figure 10c shows a positive zonal wind response starting in February and lasting through March in the lower stratosphere, in agreement with observations, whereas the average across all R-ALL ensemble members shows a weakening wind response in the lower stratosphere until mid-March (Figure 3f).

Figure 11 further compares the time evolution of the stratospheric

temperatures and winds in the R-ALL ensemble members with large tropospheric NAM response to that in all R-ALL ensemble members and observations. In all four ensemble members, the lower stratospheric wind response is positive and close to observations through March until mid-April. All four ensemble members show a negative temperature response in February, and three of them also show a negative response through most of March. Although this is qualitatively consistent with observations, the magnitude of the observed cooling is outside the range of simulated responses.

In summary we conclude that, while qualitatively the R-ALL simulations capture the downward propagation of the zonal wind anomalies to the troposphere following the strong polar vortex event in late winter and early spring, the magnitude of the observed event can only be captured if preconditioning is reproduced both in the troposphere and lower stratosphere, consistent with previous studies. However, considerably larger ensembles are necessary to study the nature of occurrence of such extremes.

4. Discussion and Conclusions

Our model experiments have been designed to answer the following question: Is the record Arctic ozone loss in 2011 the primary driver of the observed tropospheric extreme spring circulation anomalies? We find that, in the model, even an ozone anomaly of the magnitude of observed record Arctic ozone loss cannot induce a significant anomaly in the tropospheric circulation when taken in isolation from underlying meteorological conditions. This result is consistent with another recent study [*Smith and Polvani*, 2014], who did not find a statistically significant response at the surface for ozone anomaly amplitudes within the observed range. However, when the lower boundary conditions favor a reduced tropospheric wave forcing and, consequently, intensified polar vortex, the ozone anomaly amplifies the dynamical response of the stratosphere so that the response to the combined SST and ozone forcing is considerably enhanced increasing the probability of positive NAM events of large magnitude. Furthermore, our results suggest that the large magnitude of the observed tropospheric circulation anomaly in spring 2011 required a preconditioning, which is not attributable to SST or ozone anomalies and therefore, likely, a result of internal atmospheric dynamics.

The results of model experiment by *Hurwitz et al*. [2012] suggest that the positive tropospheric NAM response may be attributable to a warm North Pacific SST anomaly. Our experiments, which prescribe realistic 2010/2011 SST/SIC conditions for the whole globe, cannot be used to unambiguously attribute the response to a specific SST region. Although the relation between NAM and ENSO remains a matter of research, the La Niña conditions, which prevailed during 2011, are often linked to a positive NAM response through winter and early spring [e.g., *Greatbatch and Jung*, 2007; *Li and Lau*, 2012] and therefore could have contributed to the positive NAM response, both in the observations and in our simulations. Moreover, the North Pacific SST anomalies are themselves related to ENSO variability [*Alexander et al*., 2002]; therefore, disentangling their atmospheric signatures is not straightforward.

Our results definitely should not be interpreted as if the Arctic ozone depletion is of only a minor meteorological significance. Although such conclusion might be inferred based on the R-O3 experiment, we note that this experiment is rather unrealistic because large ozone depletion in the Arctic can only occur during exceptionally cold winters [e.g., *Rex et al*., 2006], i.e., under certain meteorological conditions favored by appropriate tropospheric forcing [*Orsolini et al*., 2009]. The significance of the Arctic ozone should therefore be inferred from the comparison of R-SST and R-ALL results. In R-SST, which can be thought as an experiment reproducing a climate without the direct effect of ozone depleting substances on the atmosphere, the impact of the stratospheric anomalies on the troposphere is considerably weaker than that in R-ALL, indicating the importance of Arctic ozone depletion. Moreover, the responses to SST and ozone in the stratosphere are nonadditive, likely due to nonlinear interactions between the dynamical impacts of SST and ozone forcings, which may be also interpreted as that the atmospheric response to ozone forcing depends on the background meteorological conditions upon which the forcing is applied.

Our study has several limitations, which needs to be kept in mind. First, the lack of chemical coupling may lead to an underestimation of atmospheric response to ozone response. *Gabriel et al*. [2007] and *Gillett et al*. [2009] have found significant impacts of ozone zonal asymmetries on the dynamics not accounted for in our experiments. However, these responses mainly appear in the stratosphere, and their impacts on the tropospheric climate have not been detected so far. Second, only one model (ECHAM-5) is used in this study;

thus, it would be desirable to repeat the calculations with another model to assess the robustness of the ECHAM5 findings.

There are several implications of our results. First, extended weather prediction models, even when capturing the stratospheric response to tropospheric forcing, may underestimate stratosphere-troposphere coupling if not accounting for potential chemical ozone depletion. Second, chemical ozone perturbations in the Arctic not associated with meteorological conditions is unlikely to induce considerable impact on tropospheric dynamics. This, in particular, concerns the expected Arctic ozone layer recovery whose magnitude is projected to be smaller than the anomalies used in our study [*WMO*, 2011]. Third, studies seeking to estimate the contribution of the observed Arctic ozone depletion to the past tropospheric changes should also include realistic lower boundary conditions.

In summary, our results indicate that ozone-climate interactions in the Arctic can be an important factor in the intraseasonal climate variability, at least during the period when ozone depleting substances in the stratosphere remain high enough to allow for large ozone loss. This result calls for the need to include interactive stratospheric chemistry into extended weather and seasonal prediction models.

Acknowledgments
We thank Lorenzo Polvani and two anonymous reviewers for constructive comments. We also thank Lorenzo Polvani for sharing their results before publication. MERRA data used in this study have been provided by the Global Modeling and Assimilation Office (GMAO) at NASA Goddard Space Flight Center through the NASA GES DISC online archive. UK MetOffice is acknowledged for providing HadISSC data via their website www.metoffice.gov.uk/hadobs. We thank the MLS teams for providing the data used for the comparison with MERRA ozone. ECMWF is acknowledged for providing ERA-Interim data. A.Y.K. is funded by the Academy of Finland through grants 259537 and 140408. J.P.'s contribution is supported by NASA under grant NNX13AM24G.

References

Adams, C., et al. (2012), Severe 2011 ozone depletion assessed with 11 years of ozone, NO_2, and OClO measurements at 80°N, *Geophys. Res. Lett.*, *39*, L05806, doi:10.1029/2011GL050478.
Alexander, M. A., I. Blade, M. Newman, J. R. Lanzante, N.-C. Lau, and J. D. Scott (2002), The atmospheric bridge: The influence of ENSO teleconnections on air-sea interaction over the global oceans, *J. Clim.*, *15*, 2205–2231.
Arblaster, J. M., and G. A. Meehl (2006), Contributions of external forcings to southern annular mode trends, *J. Clim.*, *19*, 2896–2905.
Baldwin, M. P., and T. J. Dunkerton (2001), Stratospheric harbingers of anomalous weather regimes, *Science*, *294*, 581–584.
Black, R. X., and B. A. McDaniel (2004), Diagnostic case studies of the Northern Annular Mode, *J. Clim.*, *17*, 3990–4004.
Chen, G., and P. Zurita-Gotor (2008), The tropospheric jet response to prescribed zonal forcing in an idealized atmospheric model, *J. Atmos. Sci.*, *65*, 2254–2271, doi:10.1175/2007JAS2589.1.
Dee, D. P., et al. (2011), The ERA-Interim reanalysis: Configuration and performance of the data assimilation system, *Q. J. R. Meteorol. Soc.*, *137*, 553–597, doi:10.1002/qj.828.
Deser, C., and A. S. Phillips (2009), Atmospheric circulation trends, 1950–2000: The relative roles of sea surface temperature forcing and direct atmospheric radiative forcing, *J. Clim.*, *22*, 396–413.
Fortuin, J. P. F., and H. Kelder (1998), An ozone climatology based on ozondesonde and satellite measurements, *J. Geophys. Res.*, *103*, 31,709–31,734, doi:10.1029/1998JD200008.
Gabriel, A., D. Peters, I. Kirchner, and H.-F. Graf (2007), Effect of zonally asymmetric ozone on stratospheric temperature and planetary wave propagation, *Geophys. Res. Lett.*, *34*, L06807, doi:10.1029/2006GL028998.
Gillett, N. P., and D. W. J. Thompson (2003), Simulation of recent Southern Hemisphere climate change, *Science*, *302*, 273–275, doi:10.1126/science.1087440.
Gillett, N. P., M. R. Allen, and K. D. Williams (2003), Modelling the atmospheric response to doubled CO2 and depleted stratospheric ozone using a stratosphere-resolving coupled GCM, *Q. J. R. Meteorol. Soc.*, *129*, 947–966.
Gillett, N. P., J. F. Scinocca, D. A. Plummer, and M. C. Reader (2009), Sensitivity of climate to dynamically consistent zonal asymmetries in ozone, *Geophys. Res. Lett.*, *36*, L10809, doi:10.1029/2009GL037246.
Graf, H.-F., I. Kirchner, and J. Perlwitz (1998), Changing lower stratospheric circulation: The role of ozone and greenhouse gases, *J. Geophys. Res.*, *103*, 11,251–11,261, doi:10.1029/98JD00341.
Greatbatch, R. J., and T. Jung (2007), Local versus tropical diabatic heating and the winter North Atlantic oscillation, *J. Clim.*, *20*, 2058–2075.
Hartmann, D. L., J. M. Wallace, V. Limpasuvan, D. W. J. Thompson, and J. R. Holton (2000), Can ozone depletion and global warming interact to produce rapid climate change, *Proc. Natl. Acad. Sci. U.S.A.*, *97*, 1412–1417.
Hoerling, M. P., J. W. Hurrell, and T. Xu (2001), Tropical origins for recent North Atlantic climatic change, *Science*, *292*, 90–92.
Hu, Y. Y., and Y. Xia (2013), Extremely cold and persistent stratospheric Arctic vortex in the winter of 2010–2011, *Chin. Sci. Bull.*, *58*(3155), 3160, doi:10.1007/s11434-013-5945-5.
Hurrell, J. W. (1995), Decadal trends in the North Atlantic oscillation: Regional temperatures and precipitation, *Science*, *269*, 676–679.
Hurrell, J. W., J. J. Hack, D. Shea, J. M. Caron, and J. Rosinski (2008), A new sea surface temperature and sea ice boundary dataset for the Community Atmosphere Model, *J. Clim.*, *21*, 5145–5153, doi:10.1175/2008JCLI2292.1.
Hurwitz, M. M., P. A. Newman, and C. I. Garfinkel (2011), The Arctic vortex in March 2011: A dynamical perspective, *Atmos. Chem. Phys.*, *11*, 11,447–11,453, doi:10.5194/acp-11-11447-2011.
Hurwitz, M. M., P. A. Newman, and C. I. Garfinkel (2012), On the influence of North Pacific sea surface temperature on the Arctic winter climate, *J. Geophys. Res.*, *117*, D19110, doi:10.1029/2012JD017819.
Karpechko, A. Yu., N. P. Gillett, G. J. Marshall, and A. A. Scaife (2008), Stratospheric influence on circulation changes in the Southern Hemisphere troposphere in coupled climate models, *Geophys. Res. Lett.*, *35*, L20806, doi:10.1029/2008GL035354.
Kindem, I. T., and B. Christiansen (2001), Tropospheric response to stratospheric ozone loss, *Geophys. Res. Lett.*, *28*, 1547–1550, doi:10.1029/2000GL012552.
Kodera, K., and H. Koide (1997), Spatial and seasonal characteristics of recent decadal trends in the northern hemispheric troposphere and stratosphere, *J. Geophys. Res.*, *102*(D16), 19,433–19,447, doi:10.1029/97JD01270.
Kodera, K., and K. Yamazaki (1994), A possible influence of recent polar stratospheric coolings on the troposphere in the Northern Hemisphere winter, *Geophys. Res. Lett.*, *21*, 809–812, doi:10.1029/94GL00513.
Kuroda, Y. (2008), Effect of stratospheric sudden warming and vortex intensification on the tropospheric climate, *J. Geophys. Res.*, *113*, D15110, doi:10.1029/2007JD009550.

Kuroda, Y., and K. Kodera (1999), Role of planetary waves in the stratosphere-troposphere coupled variability in the Northern Hemisphere winter, *Geophys. Res. Lett.*, *26*, 2375–2378, doi:10.1029/1999GL900507.
Langematz, U., M. Kunze, K. Krüger, K. Labitzke, and G. L. Roff (2003), Thermal and dynamical changes of the stratosphere since 1979 and their link to ozone and CO2 changes, *J. Geophys. Res.*, *108*(D1), 4027, doi:10.1029/2002JD002069.
Li, Y., and N.-C. Lau (2012), Influences of ENSO on stratospheric variability, and the descent of stratospheric perturbations into the lower troposphere, *J. Clim.*, *26*, 4725–4748, doi:10.1175/JCLI-D-12-00581.1.
Limpasuvan, V., and D. L. Hartmann (2000), Wave-maintained annular modes of climate variability, *J. Clim.*, *13*, 4414–4429.
Limpasuvan, V., D. L. Hartmann, D. W. J. Thompson, K. Jeev, and Y. L. Yung (2005), Stratosphere-troposphere evolution during polar vortex intensification, *J. Geophys. Res.*, *110*, D24101, doi:10.1029/2005JD006302.
Manney, G. L., et al. (2011), Unprecedented Arctic ozone loss in 2011, *Nature*, *478*, 469–475, doi:10.1038/nature10556.
Manzini, E., M. A. Giorgetta, M. Esch, L. Kornblueh, and E. Roeckner (2006), The influence of sea surface temperatures on the northern winter stratosphere: Ensemble simulations with the MAECHAM5 model, *J. Clim.*, *19*, 3863–3881, doi:10.1175/JCLI3826.1.
McLandress, C., T. G. Shepherd, J. F. Scinocca, D. A. Plummer, M. Sigmond, A. I. Jonsson, and M. C. Reader (2011), Separating the dynamical effects of climate change and ozone depletion. Part II: Southern Hemisphere troposphere, *J. Clim.*, *24*, 1850–1868, doi:10.1175/2010JCLI3958.1.
Morgenstern, O., et al. (2010), Anthropogenic forcing of the Northern Annular Mode in CCMVal-2 models, *J. Geophys. Res.*, *115*, D00M03, doi:10.1029/2009JD013347.
Newman, P. A., E. R. Nash, and J. E. Rosenfield (2001), What controls the temperature of the Arctic stratosphere during the spring?, *J. Geophys. Res.*, *106*, 19,999–20,010.
Omrani, N.-E., N. Keenlyside, J. Bader, and E. Manzini (2014), Stratosphere key for wintertime atmospheric response to warm Atlantic decadal conditions, *Clim. Dyn.*, *42*, 649–663, doi:10.1007/s00382-013-1860-3.
Orsolini, Y. J., A. Y. Karpechko, and G. Nikulin (2009), Variability of the Northern Hemisphere polar stratospheric cloud potential: The role of North Pacific disturbances, *Q. J. R. Meteorol. Soc.*, *135*, 1020–1029.
Perlwitz, J., S. Pawson, R. L. Fogt, J. E. Nielsen, and W. D. Neff (2008), Impact of stratospheric ozone hole recovery on Antarctic climate, *Geophys. Res. Lett.*, *35*, L08714, doi:10.1029/2008GL033317.
Perlwitz, J., M. Hoerling, J. Eischeid, T. Xu, and A. Kumar (2009), A strong bout of natural cooling in 2008, *Geophys. Res. Lett.*, *36*, L23706, doi:10.1029/2009GL041188.
Rayner, N. A., D. E. Parker, E. B. Horton, C. K. Folland, L. V. Alexander, D. P. Rowell, E. C. Kent, and A. Kaplan (2003), Global analyses of sea surface temperature, sea ice, and night marine air temperature since the late nineteenth century, *J. Geophys. Res.*, *108*(D14), 4407, doi:10.1029/2002JD002670.
Rex, M., et al. (2006), Arctic winter 2005: Implications for stratospheric ozone loss and climate change, *Geophys. Res. Lett.*, *33*, L23808, doi:10.1029/2006GL026731.
Rienecker, M., et al. (2011), MERRA: NASA's Modern-Era Retrospective analysis for research and applications, *J. Clim.*, *24*, 3624–3648, doi:10.1175/JCLI-D-11-00015.1.
Roeckner, E., R. Brokopf, M. Esch, M. Giorgetta, S. Hagemann, L. Kornblueh, E. Manzini, U. Schlese, and U. Schulzweida (2006), Sensitivity of simulated climate to horizontal and vertical resolution in the ECHAM5 atmosphere model, *J. Clim.*, *19*, 3771–3791, doi:10.1175/JCLI3824.1.
Salby, M., and P. Callaghan (2007), On the wintertime increase of arctic ozone: Relationship to changes of the polar-night vortex, *J. Geophys. Res.*, *112*, D06116, doi:10.1029/2006JD007948.
Sexton, D. M. H. (2001), The effect of stratospheric ozone depletion on the phase of the Antarctic oscillation, *Geophys. Res. Lett.*, *28*(19), 3697–3700, doi:10.1029/2001GL013376.
Shaw, T. A., and J. Perlwitz (2013), The life cycle of Northern Hemisphere downward wave coupling between the stratosphere and troposphere, *J. Clim.*, *26*, 1745–1763, doi:10.1175/JCLI-D-12-00251.1.
Shindell, D. T., R. L. Miller, G. A. Schmidt, and L. Pandolfo (1999), Simulation of recent northern winter climate trends by greenhouse gas forcing, *Nature*, *399*, 452–455.
Shindell, D. T., G. A. Schmidt, R. L. Miller, and D. Rind (2001), Northern Hemisphere winter climate response to greenhouse gas, ozone, solar, and volcanic forcing, *J. Geophys. Res.*, *106*(D7), 7193–7210, doi:10.1029/2000JD900547.
Smith, K., and L. Polvani (2014), The surface impacts of Arctic stratospheric ozone anomalies, *Environ. Res. Lett.*, in press.
Solomon, S., R. W. Portmann, and D. W. J. Thompson (2007), Contrasts between Antarctic and Arctic ozone depletion, *Proc. Natl. Acad. Sci. U.S.A.*, *104*, 445–449.
Son, S.-W., L. M. Polvani, D. W. Waugh, H. Akiyoshi, R. Garcia, D. Kinnison, S. Pawson, E. Rozanov, T. G. Shepherd, and K. Shibata (2008), The impact of stratospheric ozone recovery on the Southern Hemisphere westerly jet, *Science*, *320*, 1486–1489, doi:10.1126/science.1155939.
Stott, P. A., M. Allen, N. Christidis, R. M. Dole, M. Hoerling, C. Huntingford, P. Pall, J. Perlwitz, and D. Stone (2013), Attribution of weather and climate-related events, in *Climate Science for Serving Society: Research, Modeling and Prediction Priorities*, edited by G. R. Asrar and J. W. Hurrell, pp. 307–337, Springer, Dordrecht.
Thompson, D. W. J., and S. Solomon (2002), Interpretation of recent Southern Hemisphere climate change, *Science*, *296*, 895–899, doi:10.1126/science.1069270.
Thompson, D. W. J., and J. M. Wallace (2000), Annular modes in the extratropical circulation. Part I: Month-to-month variability, *J. Clim.*, *13*, 1000–1016.
Trenberth, K. E., G. W. Branstator, D. Karoly, A. Kumar, N. Lau, and C. Ropelewski (1998), Progress during TOGA in understanding and modeling global teleconnections associated with tropical sea surface temperatures, *J. Geophys. Res.*, *103*, 14,291–14,324, doi:10.1029/97JC01444.
Volodin, E. M., and V. Y. Galin (1998), Sensitivity of midlatitude Northern Hemisphere winter circulation to ozone depletion in the lower stratosphere, *Russ. Meteor. Hydrol.*, *8*, 23–32.
Waters, J. W., et al. (2006), The Earth Observing System Microwave Limb Sounder (EOS MLS) on the Aura satellite, *IEEE Trans. Geosci. Remote Sens.*, *44*, 1075–1092, doi:10.1109/TGRS.2006.873771.
World Meteorological Organization (WMO) (2003), *Scientific Assessment of Ozone Depletion: 2002, Rep. 47*, Global Ozone Res. and Monit. Proj., 498 pp., World Meteorol. Organ., Geneva, Switzerland.
World Meteorological Organization (WMO) (2007), *Scientific Assessment of Ozone Depletion: 2006, Rep. 50*, Global Ozone Res. and Monit. Proj., 572 pp., World Meteorol. Organ., Geneva, Switzerland.
World Meteorological Organization (WMO) (2011), *Scientific Assessment of Ozone Depletion: 2010, Rep. 52*, Global Ozone Res. Monit. Proj., 516 pp., World Meteorol. Organ., Geneva, Switzerland.